

The orientation dependence of quasar single-epoch black hole mass scaling relationships

Jessie C. Runnoe¹*, M. S. Brotherton¹, Z. Shang², B. J. Wills³, and M. A. DiPompeo¹

¹Department of Physics and Astronomy, University of Wyoming, Laramie, WY 82071, USA

²Department of Physics, Tianjin Normal University, Tianjin 300074, China

³Department of Astronomy, University of Texas, Austin, TX 78712, USA

Preprint 2012 July 05

ABSTRACT

Black hole masses are estimated for radio-loud quasars using several self-consistent scaling relationships based on emission-line widths and continuum luminosities. The emission lines used, H β , Mg II λ 2798, and C IV λ 1549, have different dependencies on orientation as estimated by radio core dominance. We compare differences in the log of black hole masses estimated from different emission lines and show that they depend on radio core dominance in the sense that core-dominated, jet-on objects have systematically smaller H β and Mg II determined masses compared to those from C IV, while lobe-dominated edge-on objects have systematically larger H β and Mg II determined masses compared to those from C IV. The effect is consistent with the H β line width, and to a lesser extent that of Mg II, being dependent upon orientation in the sense of a axisymmetric velocity field plus a projection effect. The size of the effect is nearly an order of magnitude in black hole mass going from one extreme orientation to the other. We find that radio spectral index is a good proxy for radio core dominance and repeating this analysis with radio spectral index yields similar results. Accounting for orientation could in principle significantly reduce the scatter in black hole mass scaling relationships, and we quantify and offer a correction for this effect cast in terms of radio core dominance and radio spectral index.

Key words: galaxies: active quasars: general accretion, accretion discs black hole physics.

1 INTRODUCTION

Black hole mass is an important fundamental quasar parameter that can be measured directly via reverberation mapping, which probes the motions of gas in the vicinity of the black hole (Blandford & McKee 1982; Peterson 1993). If the motion of gas in the broad line region (BLR) is dominated by the gravitational potential of the black hole, then the central mass can be estimated from the scaled virial product,

$$M_{BH} = f \frac{\Delta V^2 R}{G}, \quad (1)$$

where G is the gravitational constant, R is the distance to the broad line region gas that has velocity dispersion ΔV , and f is a scale factor of order unity that contains unknown information about the BLR geometry and orientation effects.

The factor f may vary between objects and possi-

bly even between emission lines in the same object, but determining f for individual objects requires an independent measure of the black hole mass. Instead, a measure of the statistical scale factor, $\langle f \rangle$, is borrowed from the $M_{BH} - \sigma_*$ relationship for quiescent galaxies in order to calibrate the zero-point of the reverberation mapping masses. One recent measurement of the statistical scale factor yields $\langle f \rangle = 5.25 \pm 1.21$ (Woo et al. 2010).

Reverberation mapping then measures the central black hole mass by combining emission-line width (ΔV) and the size of the BLR (R_{BLR}), inferred from the time delay in an emission line ($R_{BLR} = c\tau$). At present, reverberation mapping black hole masses have been measured for approximately 50 active galactic nuclei (AGN) (e.g., Peterson et al. 2004; Bentz et al. 2009; Grier et al. 2012).

Another important result has followed from reverberation mapping: the radius-luminosity ($R - L$) relationship. The time lag for emission lines to respond to variation in the continuum is longer in more luminous objects (Kaspi et al. 2000, 2005), such that $R_{BLR} \propto L^{1/2}$ when host galaxy contamination is removed (Bentz et al. 2009). This result is

* E-mail: jrunnoe@uwyo.edu

based on measurements of $\text{H}\beta$, but limited CIV -based results are consistent with this relationship (Kaspi et al. 2007).

The $R - L$ relationship anchors the single-epoch “mass scaling relationships,” which provide an indirect estimate of black hole mass. The mass scaling relationships are widely used because they can be applied to any object with a single-epoch optical/ultra-violet (UV) spectrum measurement of a broad emission-line width and continuum luminosity, the proxy for the BLR radius. The velocity dispersion is usually measured, for $\text{H}\beta$, $\text{Mg}\text{II} \lambda 2798$, or $\text{C}\text{IV} \lambda 1549$, either from the full width at half maximum (FWHM) or the second moment of the line, σ_{line} , called the line dispersion. The two line measurements have different characteristics and advantages, though σ_{line} may be preferred (Collin et al. 2006; Peterson 2011). We focus on the FWHM line measurement in order to facilitate comparisons with older studies and save an investigation of σ_{line} for future work.

Multiple studies have shown that the $\text{H}\beta$ FWHM measurements used to estimate black hole mass depend on orientation. Radio core dominance (R), the ratio of the radio core flux density to the extended radio lobe flux density at 5 GHz rest-frame, is related to the angle between the radio axis and the line of sight in the beaming model for radio sources (e.g., Scheuer & Readhead 1979; Orr & Browne 1982; Ghisellini et al. 1993). Wills & Browne (1986) found that the FWHM of $\text{H}\beta$ was significantly correlated with radio core dominance such that there is an absence of very broad widths for objects with large core dominance. Their result is consistent with the motion of the $\text{H}\beta$ -emitting gas being primarily in a plane perpendicular to the radio axis. McLure & Dunlop (2001) test such a disc model for the BLR and find that it is a good fit to observations for $\text{H}\beta$.

The relationship between broad-line FWHM and core dominance found for $\text{H}\beta$ has also been investigated for other broad lines, sometimes using radio spectral index as a proxy for radio core dominance. Radio spectral index and radio core dominance are well correlated (Brotherton 1996; Jarvis & McLure 2006) but it should be noted that radio spectral index is neither the same as radio core dominance nor a perfect measure of orientation (e.g., DiPompeo et al. 2012). Jarvis & McLure (2006) and Fine et al. (2011) find that the FWHM of MgII has an orientation dependence weaker than that of $\text{H}\beta$ and Fine et al. (2011) find no orientation dependence for the FWHM of CIV , where radio spectral index is used to indicate orientation. This result for CIV is consistent with the result from Vestergaard et al. (2000) that FWHM CIV does not correlate with radio core dominance.

Given the orientation dependence of FWHM for the broad emission lines used to estimate black hole mass, it has been suggested that black hole estimates based on single-epoch scaling relationships will depend on orientation (e.g., Baskin & Laor 2005; Jarvis & McLure 2006). Black hole masses cannot be as accurately estimated without ΔV (Assef et al. 2012), so we investigate the dependence of black hole mass estimates on radio core dominance for the radio-loud (RL) subsample from the Shang et al. (2011) spectral energy distribution (SED) atlas.

In Section 2 we provide sample data and discuss spectral fitting and black hole mass estimates. Section 3 confirms the correlations between FWHM and radio core dominance and presents the correlations between differences in the log

of black hole mass estimates and radio core dominance. Here we also provide corrections to black hole mass based on the radio core dominance. To conclude Section 3, the analysis is repeated for radio spectral index. The correlations between differences in the log of black hole mass estimated from different emission lines and radio core dominance are discussed in Section 4 and Section 5 summarizes our investigation and corrections to black hole mass.

Black hole masses and luminosities are calculated using a cosmology with $H_0 = 70 \text{ km s}^{-1} \text{ Mpc}^{-1}$, $\Omega_\Lambda = 0.7$, and $\Omega_m = 0.3$.

Because we employ several values of “ R ” in this study, we explicitly state the definition of each parameter here to avoid confusion. Radio core dominance, R , is the ratio of the core flux density to the lobe flux density at 5 GHz rest frame. The ratio of the core luminosity at 5 GHz rest frame to the optical V-band luminosity, R_V , is another measure of core dominance (Wills & Brotherton 1995). Radio loudness, R^* , is the ratio of the total radio luminosity at 5 GHz rest frame to the optical luminosity (Stocke et al. 1992). The radio spectral index, α ($f_\nu \sim \nu^\alpha$), is a slope between two or more radio frequencies.

2 SAMPLE, DATA, AND MEASUREMENTS

For this investigation, we use the RL subsample of the Shang et al. (2011) SED atlas. See Wills et al. (1995) or Netzer et al. (1995) for additional sample details. Many of the blazars originally included in this sample have been excluded from this investigation. 4C 11.69, which was identified as a blazar by Runnoe et al. (2012b) based on infrared variability, has also been excluded. Our final sample has 52 objects.

Originally assembled to study orientation, sample members were selected to have similar extended radio luminosity, which is thought to be isotropic. Thus, objects in the sample are similar to each other but viewed at different angles indicated by their radio core luminosities. While this selection was compromised by the original spherical aberration problem with Hubble Space Telescope, requiring selection of brighter targets, the extended radio luminosities are similar with a limited range versus $\log R$ (Figure 1, left), and variation in radio core luminosity is therefore largely responsible for variation in $\log R$ (right).

We calculate radio core dominance, the ratio of the flat-spectrum core to the steep-spectrum extended lobes at 5 GHz rest frame, for the sample. The radio data from the Shang et al. (2011) SEDs are insufficient for this calculation, so we assembled radio core and total flux densities from high quality surveys and the literature. We applied a k-correction to the radio fluxes assuming slopes of $\alpha = 0$ and $\alpha = -0.7$ for the core and lobes, respectively. We also calculate the orientation indicator $\log R_V$, the 5 GHz core flux density to the optical V-band flux density.

We calculate radio spectral index for our sample in order to provide an orientation measure that may be easier to obtain and can be measured in some cases when $\log R$ cannot. We use the convention $f_\nu \sim \nu^\alpha$, where f_ν is the radio flux, ν is the frequency, and α is the radio spectral index. We measure the slope in two ways from the radio data in the Shang et al. (2011) SEDs. α_{all} is the radio spectral index

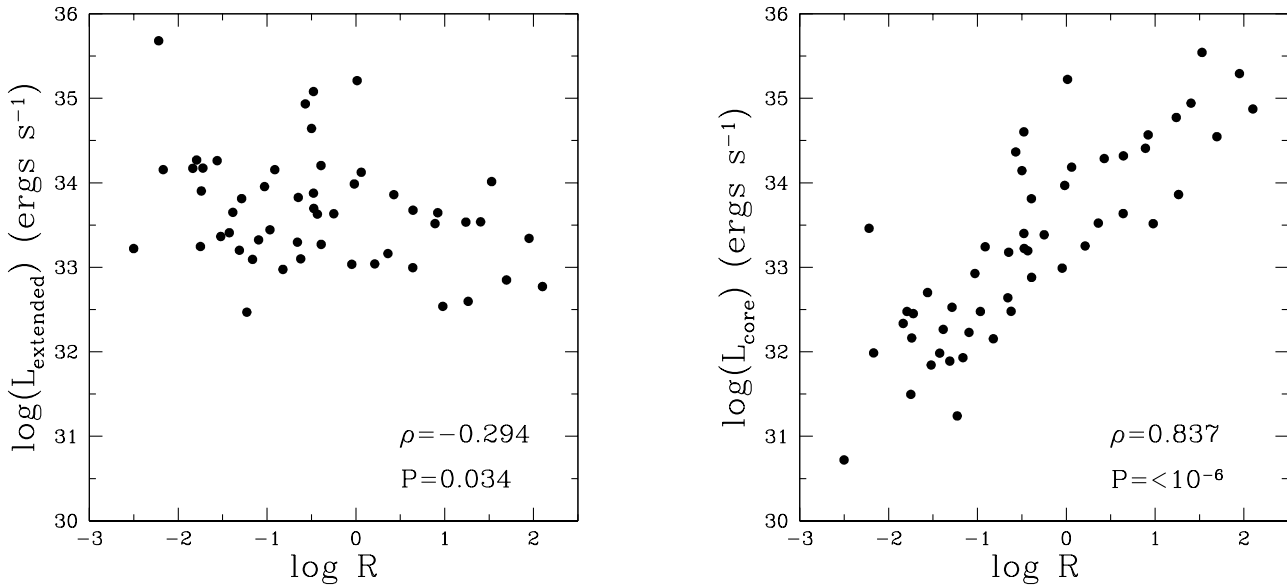


Figure 1. Core and extended radio luminosities versus $\log R$. The success of selecting objects with similar extended luminosities is apparent in the left panel, so variation in $\log R$ is due primarily to variation in the radio core luminosity seen in the right panel.

measured by fitting a line to all of the available radio data in logarithmic space. $\alpha_{4.9}^{1.4}$ is the radio spectral index measured from two data points at observed-frame 1.4 GHz and 4.9 GHz. We include this second measure in order to avoid the turnover of the radio spectrum around 1 GHz that is due to synchrotron self absorption and does not reflect the orientation of the object. We do note that we do not observe such a turnover in most of our objects; most are well fit with a single line using all of the available radio data from the SEDs.

Table 1 lists radio properties for the sample. It is arranged as follows:

Column (1) gives the object name.

Column (2) gives the redshift from Shang et al. (2011).

Column (3) gives the frequency at which fluxes were observed for the core and total radio components, respectively. In cases where the extended radio flux was observed instead of the total, the frequency of this observation is listed in Column (3).

Columns (4) and (5) give the k-corrected, 5 GHz rest-frame flux densities in mJy. In most cases, the extended flux is calculated from measurements of the core and total flux, but in some cases the extended and core emission were the quantities directly listed in the reference. The cases where extended emission is actually observed rather than calculated are indicated in Column 5.

Column (6) gives the log of the k-corrected, rest-frame, radio core dominance, $\log R$.

Column (7) gives the radio loudness parameter, $\log R^*$, where Shang et al. (2011) calculates $R^* = f(5 \text{ GHz})/f(4215 \text{ \AA})$ in the rest frame.

Column (8) gives the reference for the radio data used to calculate radio core dominance. Radio spectral index is always calculated from the radio portion of the Shang et al. (2011) SEDs.

Spectral fitting to measure emission-line widths and

continuum luminosities was carried out by Tang et al. (2012) following the prescription of Shang et al. (2007). Tang et al. fit the optical/UV region of the SEDs using SPECFIT (Kriss 1994). They model the regions around C IV $\lambda 1549$, Mg II $\lambda 2798$, and H β each with a power-law continuum and a line profile of two Gaussian components. A third Gaussian, that is not included in the total FWHM of the line profile, is added to the H β profile to fit the contribution to emission from the narrow-line region. The C IV line does not have a strong contribution from the narrow-line region (Wills et al. 1993) and, while Mg II does sometimes have such a component, it is not apparent in our objects. Optical and UV Fe II emission is modeled with templates (Boroson & Green 1992; Vestergaard & Wilkes 2001) based on the Seyfert 1 galaxy, I Zw1, that are allowed to vary in amplitude and velocity width. Continuum luminosities based on flux measurements from these fits are from Runnoe et al. (2012a). The resulting FWHM values for H β , C IV, and Mg II, the bolometric luminosity, and other relevant data are given in Table 2

Tang et al. (2012) estimate black hole masses for the Shang et al. atlas using single-epoch scaling relationships from Vestergaard & Peterson (2006) for H β and C IV and from Vestergaard & Osmer (2009) for Mg II. Multiple lines are used to statistically approach the true black hole mass and these scaling relationships were chosen specifically because they are self-consistent (Vestergaard et al. 2011), thus enabling meaningful comparisons among them. The optical/UV region of our SEDs facilitates consistent estimates of black hole mass from different broad emission lines because they each have quasi-simultaneous data and coverage over a large enough wavelength range to include H β , Mg II, and C IV. Black hole masses are listed in Table 2.

Not all measurements are available for all objects. There are 38 (73%) objects with measurements of $\log R$, $\text{FWHM}_{\text{H}\beta}$, and FWHM_{CIV} , 39 (75%) objects with mea-

Table 1. Radio data

Object	Redshift	ν_{core}/ν_{tot}^a (GHz)/(GHz)	f_{core} (mJy)	f_{ex} (mJy)	$\log R$	$\log R^*$	Reference	α_{all}^d	$\alpha_{4.9}^{1.4} e$
3C 110	0.7749	4.85/ 4.85	33.38	33.63	-0.25	2.68	8	-0.99	-0.65
3C 175	0.7693	8.47/ 4.86	32.34	34.17	-1.84	2.99	2,9	-1.02	-1.10
3C 186	1.0630	1.70/ 1.70	34.19	34.12	0.06	3.33	14	-1.20	-1.18
3C 207	0.6797	4.86/ 1.40	33.81	34.20	-0.39	3.63	2,12	-0.67	-0.65
3C 215	0.4108	4.89/ 4.89	31.84	33.36	-1.52	3.37	6	-0.99	-1.00
3C 232	0.5297	8.55/ 8.55	33.64	33.00	0.64	2.87	7	-0.51	-0.41
3C 254	0.7363	5.00/ 5.00	32.45	34.17	-1.72	3.71	11	-1.06	-1.25
3C 263	0.6464	5.00/ 4.85	33.24	34.16	-0.91	3.00	2,9	-0.87	-0.90
3C 277.1	0.3199	1.70/ 1.70	31.98	33.41	-1.43	3.53	11	-0.76	-0.87
3C 281	0.6017	1.40/ 1.40	32.48	33.44	-0.97	3.23	10	-0.88	-0.85
3C 288.1	0.9631	5.00/ 5.00	31.99	34.16	-2.17	3.42	11	-0.96	-1.07
3C 334	0.5553	1.40/ 1.40	33.18	33.83	-0.65	3.11	12	-0.87	-0.83
3C 37	0.6661	5.00/ 5.00	33.20	33.63	-0.43	3.74	10	-0.85	-0.79
3C 446	1.4040	1.40/ 1.40	35.54	34.01 ^b	1.53	4.34	1	-0.32	-0.11
3C 47	0.4250	4.89/ 4.89	32.53	33.81	-1.29	3.82	6	-0.96	-0.93
4C 01.04	0.2634	5.00/ 5.00	32.48	33.10	-0.62	3.41	13	-0.54	-0.48
4C 06.69	1.0002	1.40/ 1.40	34.87	32.77 ^b	2.10	3.32	1	0.16	0.37
4C 10.06	0.4075	4.99/ 4.99	32.64	33.30	-0.66	2.67	18	-0.79	-0.96
4C 12.40	0.6836	5.00/ 5.00	31.93	33.09 ^b	-1.16	3.03	16	-0.97	-0.99
4C 19.44	0.7192	1.40/ 1.40	34.29	33.86	0.43	3.42	12	-0.44	-0.03
4C 20.24	1.1135	1.40/ 1.40	34.14	34.64	-0.50	3.62	12	-0.52	-0.39
4C 22.26	0.9760	1.40/ 1.40	32.93	33.95	-1.03	3.26	12	-0.92	-1.03
4C 30.25	1.0610	1.40/ 1.40	32.16	33.90	-1.74	2.92	12	-0.91	-1.07
4C 31.63	0.2952	1.40/ 1.40	33.52	32.54	0.98	2.93	1	-0.15	0.00
4C 39.25	0.6946	15.00/ 15.00	33.46	35.68 ^b	-2.22	3.65	3	0.08	0.75
4C 40.24	1.2520	15.00/ 15.00	34.60	35.08	-0.48	3.94	3	-0.19	-0.01
4C 41.21	0.6124	1.40/ 1.40	33.40	33.88	-0.48	2.91	12	-0.79	0.36
4C 49.22	0.3333	0.40/ 0.40	32.99	33.04	-0.05	3.36	3	-0.64	-0.60
4C 55.17	0.8990	1.40/ 1.40	34.77	33.53	1.24	3.74	12	-0.32	-0.44
4C 58.29	1.3740	1.40/ 1.40	32.70	34.26	-1.56	2.66	12	-0.99	-1.15
4C 64.15	1.3000	5.00/ 5.00	32.48	34.27	-1.79	3.37	11	-0.67	-0.77
4C 73.18	0.3027	1.40/ 1.40	33.86	32.60	1.26	3.20	1	-0.14	-0.06
B2 0742+31	0.4616	1.40/ 1.40	33.52	33.16 ^b	0.36	2.77	12	-0.60	-0.28
B2 1351+31	1.3260	5.00/ 5.00	33.22	33.70	-0.47	2.95	17	-0.79	-0.80
B2 1555+33	0.9420	1.40/ 1.40	33.25	33.04	0.21	2.99	12	-0.52	-0.55
B2 1611+34	1.3945	15.00/ 15.00	35.22	35.21	0.01	3.77	3	0.00	-0.34
MC2 0042+101	0.5870	1.40/ 1.40	32.15	32.98	-0.82	2.92	10	-0.87	-0.78
MC2 1146+111	0.8614	5.00/ 5.00	31.89	33.20	-1.31	2.55	16	-0.86	-0.91
OS 562	0.7506	15.00/ 15.00	34.41	33.52	0.89	3.35	3	-0.08	0.24
PG 1100+772	0.3114	4.89/ 4.89	32.23	33.32	-1.10	2.65	6	-0.84	-1.00
PG 1103-006	0.4234	1.40/ 1.40	32.88	33.27	-0.39	2.94	12	-0.67	-0.55
PG 1226+023	0.1576	1.40/ 1.40	34.32	33.68	0.64	3.22	12	-0.19	-0.21
PG 1545+210	0.2642	1.40/ 1.40	31.50	33.25	-1.75	3.00	12	-0.74	-0.77
PG 1704+608	0.3730	1.40/ 1.40	32.27	33.65	-1.39	2.82	12	-0.76	-0.83
PG 2251+113	0.3253	5.00/ 5.00	30.72	33.22	-2.50	2.46	15	-0.78	-0.83
PKS 0112-017	1.3743	15.00/ 15.00	34.37	34.93	-0.57	3.45	3	0.13	0.23
PKS 0403-13	0.5700	1.40/ 1.40	34.55	32.85	1.70	3.73	1	-0.36	-0.35
PKS 0859-14	1.3320	4.90/ 4.90	34.94	33.54 ^b	1.40	3.43	8	-0.24	-0.29
PKS 1127-14	1.1870	1.66/ 1.66	35.29	33.34	1.95	3.88	4	0.04	-0.21
PKS 1656+053	0.8890	5.00/ 5.00	33.97	33.99 ^b	-0.02	3.10	5	-0.19	-0.00
PKS 2216-03	0.8993	1.40/ 1.40	34.57	33.65	0.92	3.23	1	-0.08	0.13
TEX 1156+213	0.3480	1.40/ 1.40	31.24	32.47 ^b	-1.23	2.38	12	-0.75	-0.79

^a Frequencies are observed-frame. Fluxes, $\log R$, and R^* are k-corrected to 5 GHz and in the rest-frame.^b Extended radio flux was observed rather than calculated from total and core radio fluxes.^c **References:** (1) Cooper et al. (2007); (2) Mullin et al. (2006); (3) Kovalev et al. (2005); (4) Stanghellini et al. (2005); (5) Scott et al. (2004); (6) Gilbert et al. (2004); (7) Fey & Charlton (2000); (8) Reid et al. (1999); (9) Dennett-Thorpe et al. (1997); (10) Hutchings et al. (1996); (11) Reid et al. (1995); (12) Becker et al. (1995); (13) Lister et al. (1994); (14) Spencer et al. (1991); (15) Kellermann et al. (1989); (16) Hutchings et al. (1988); (17) Rogora et al. (1986); (18) Miley & Hartraijker (1978).^d Radio spectral index measured from all radio data available in Shang et al. (2011) SEDs.^e Radio spectral index measured between observed-frame 1.4 and 4.9 GHz.

surements of $\log R$, $\text{FWHM}_{\text{H}\beta}$, and $\text{FWHM}_{\text{Mg II}}$, and 51 (98%) objects with measurements of $\log R$, $\text{FWHM}_{\text{C IV}}$, and $\text{FWHM}_{\text{Mg II}}$.

3 ANALYSIS

We investigate the dependence of the difference between the log of the black hole masses estimated with different scaling relationships on radio core dominance. We first demonstrate the relationship between FWHM and radio core dominance for $\text{H}\beta$, Mg II , and C IV , and then proceed to characterize the dependence this creates in black hole masses derived using scaling relationships calibrated for each of these emission lines. We then repeat the analysis for radio spectral index.

3.1 The orientation dependence of broad-line widths

The scatter between black hole masses estimated from different emission lines that results from varying radio core dominance is derived largely from the broad-line FWHM dependence on radio core dominance. Figure 2 shows $\log R$ versus FWHM for all three broad emission lines, where $\log R$ is on the y-axis for an easy comparison with previous results. We confirm that $\text{H}\beta$ has the strongest $\log R$ dependence, followed by Mg II , and finally C IV which shows no dependence on radio core dominance. The given correlation coefficients are Spearman rank correlation coefficients and the probability of finding these distributions of points by chance are listed in each panel.

3.2 The orientation dependence of black hole masses

The radio core dominance dependence of broad-line FWHM for $\text{H}\beta$ and Mg II implies that black hole masses estimated from those lines may also have a similar dependence (Baskin & Laor 2005; Jarvis & McLure 2006). Tang et al. (2012) show that there is scatter between black hole masses estimated from different broad emission lines. We quantify the scatter around the one-to-one relationship by taking the standard deviation of the residuals in the y direction from the best fit to the parameters: around $\text{H}\beta$ and C IV is 0.40 dex, around Mg II and C IV is 0.194 dex, and around $\text{H}\beta$ and Mg II is 0.20 dex. This scatter is in part due to radio core dominance and can be reduced by applying a correction based on $\log R$.

3.2.1 Correlations

In order to investigate how different black hole mass scaling relationships might depend on radio core dominance, we correlate the difference between the log of black hole masses estimated from different scaling relationships with radio core dominance. Table 3 gives the Spearman rank correlation coefficients and corresponding two-tailed probabilities. We normalize the masses rather than simply correlating masses derived from $\text{H}\beta$, Mg II , and C IV individually with radio core dominance because we want to isolate the bias in black hole mass from orientation and avoid effects associated with the sample having a range in intrinsic black hole

Table 3. Correlations for black hole mass, $\log R$, and α_{all}

Param 1	Param 2	N	ρ^a	P ^b
$\Delta \log(M_{BH})(\text{H}\beta - \text{Mg II})$	$\log R$	39	-0.392	0.014
$\Delta \log(M_{BH})(\text{H}\beta - \text{C IV})$	$\log R$	38	-0.515	0.001
$\Delta \log(M_{BH})(\text{Mg II} - \text{C IV})$	$\log R$	51	-0.321	0.022
L_{core}	$\log R$	52	0.837	$< 10^{-6}$
L_{ext}	$\log R$	52	-0.294	0.034
$\Delta \log(M_{BH})(\text{H}\beta - \text{Mg II})$	L_{ext}	39	0.313	0.052
$\Delta \log(M_{BH})(\text{H}\beta - \text{C IV})$	L_{ext}	38	0.228	0.168
$\Delta \log(M_{BH})(\text{Mg II} - \text{C IV})$	L_{ext}	51	-0.154	0.282
$\Delta \log(M_{BH})(\text{H}\beta - \text{Mg II})$	L_{core}	39	-0.259	0.111
$\Delta \log(M_{BH})(\text{H}\beta - \text{C IV})$	L_{core}	38	-0.435	0.006
$\Delta \log(M_{BH})(\text{Mg II} - \text{C IV})$	L_{core}	51	-0.449	0.001
$\Delta \log(M_{BH})(\text{H}\beta - \text{Mg II})$	α_{all}	39	-0.426	0.007
$\Delta \log(M_{BH})(\text{H}\beta - \text{C IV})$	α_{all}	38	-0.495	0.002
$\Delta \log(M_{BH})(\text{Mg II} - \text{C IV})$	α_{all}	51	-0.340	0.015
$\log R$	α_{all}	52	0.625	$< 10^{-6}$

^a ρ is the Spearman rank correlation coefficient.

^b P is the given probability that the observed distribution of points would arise by chance.

mass, which may mask orientation effects. The caveat to this approach is that if any systematic differences between the line width measurements depend on orientation, they will be folded into our results.

Table 3 indicates that the $\log R$ dependence of $\text{H}\beta$ and Mg II FWHM is propagated to the black hole masses derived from the $\text{H}\beta$ and Mg II scaling relationships. Taking into account the number of objects available for each correlation and the probability indicated by the Spearman rank correlation test, the difference between the log of black hole masses estimated from $\text{H}\beta$ and C IV , Mg II and C IV , and $\text{H}\beta$ and Mg II is correlated with radio core dominance with a t-ratio of 3.5, 2.4, and 2.7, respectively. This correlation with radio core dominance causes a range in the difference between black hole masses estimated from different emission lines that covers nearly an order of magnitude from the most jet-on (large values of $\log R$) to the most edge-on (small values of $\log R$) objects. In practice, the actual range will depend on the range of orientations present in any given sample and uncertainty in the orientation from $\log R$.

Core and extended radio luminosities are also listed in Table 3 in order to verify the source of the correlation between $\text{H}\beta$ and Mg II -derived masses and radio core dominance. The differences $\Delta \log(M_{BH})(\text{H}\beta - \text{C IV})$ and $\Delta \log(M_{BH})(\text{Mg II} - \text{C IV})$ are more significantly correlated with core luminosity than the extended luminosity, indicating that the correlations between the mass difference and $\log R$ are due to variation in the core luminosity among objects that are intrinsically similar.

3.2.2 Regression analysis

We also performed a regression analysis in order to describe the trends with radio core dominance. The fits in this paper are made by minimizing the chi-squared statistic using MPFIT (Markwardt 2009) which employs the Levenberg-Marquardt least squares method. The uncertainties in $\log R$ are considered to be negligible compared to those in black

Table 2. Black hole masses and luminosities

Object	$\log(L_{bol})^a$ (ergs s^{-1})	FWHM _{Hβ} (km s^{-1})	FWHM _{Mg II} (km s^{-1})	FWHM _{C IV} (km s^{-1})	$\log M_{BH}(H\beta)$ M_{\odot}	$\log M_{BH}(\text{Mg II})$ M_{\odot}	$\log M_{BH}(\text{C IV})$ M_{\odot}
3C 110	46.99	12450	5645	5700	10.09	9.47	9.47
3C 175	46.91	20925	9515	6915	10.60	9.97	9.58
3C 186	46.66	...	5790	6290	...	9.35	9.35
3C 207	46.28	3505	4140	4935	8.74	8.92	8.92
3C 215	45.77	6760	6260	5605	9.04	8.92	8.72
3C 232	46.36	4655	4620	7145	9.11	9.16	9.35
3C 254	46.17	14095	6595	5205	9.89	9.27	8.96
3C 263	46.81	4970	4265	3310	9.31	9.22	8.94
3C 277.1	45.61	3835	3380	3215	8.41	8.34	8.24
3C 281	46.23	7985	5505	4865	9.38	9.10	8.93
3C 288.1	46.61	8970	4320	4015	9.63	9.06	8.93
3C 334	46.44	6345	4840	5745	9.31	9.16	9.24
3C 37	46.18	4280	4200	3360	8.62	8.72	8.39
3C 446	47.01	...	3955	3390	...	9.21	8.87
3C 47	45.97	14005	7745	5450	9.64	9.17	8.82
4C 01.04	45.44	9905	9550	6665	9.25	9.14	8.54
4C 06.69	47.30	4015	4220	5620	9.33	9.38	9.61
4C 10.06	46.48	4735	4670	3785	9.00	9.05	8.81
4C 12.40	46.17	3565	4205	5300	8.58	8.76	8.92
4C 19.44	46.91	4575	3105	2730	9.23	8.92	8.75
4C 20.24	46.92	...	4070	3525	...	9.14	8.93
4C 22.26	46.59	...	4910	5015	...	9.07	9.04
4C 30.25	46.27	...	4440	3730	...	8.87	8.67
4C 31.63	46.61	3395	4055	4840	8.78	9.07	9.21
4C 39.25	46.91	6400	5075	4775	9.51	9.33	9.21
4C 40.24	46.60	...	3650	4920	...	8.90	9.08
4C 41.21	46.75	3445	3060	3800	8.80	8.81	9.03
4C 49.22	45.99	3910	4415	4535	8.51	8.69	8.61
4C 55.17	46.46	...	3475	6420	...	8.82	9.25
4C 58.29	47.20	...	4830	5745	...	9.50	9.64
4C 64.15	46.73	...	5125	7245	...	9.29	9.52
4C 73.18	46.40	3095	3345	3560	8.66	8.81	8.73
B2 0742+31	46.46	10690	6060	4890	9.85	9.40	9.04
B2 1351+31	46.66	...	4205	3690	...	9.06	8.89
B2 1555+33	46.21	...	4650	4240	...	8.91	8.75
B2 1611+34	47.06	4795	4010	4625	9.41	9.22	9.32
MC2 0042+101	45.68	8270	6275	4195	9.21	8.97	8.43
MC2 1146+111	46.29	7835	5020	3715	9.46	9.10	8.67
OS 562	46.74	3305	3465	3470	8.86	8.93	8.92
PG 1100+772	46.46	9390	6090	4775	9.57	9.26	9.03
PG 1103-006	46.30	5270	4780	4515	9.00	9.01	8.85
PG 1226+023	46.96	3405	2935	4530	8.96	8.92	9.27
PG 1545+210	45.93	6885	5230	4560	9.12	8.94	8.71
PG 1704+608	46.49	10465	8405	4015	9.81	9.61	8.87
PG 2251+113	46.35	4060	4110	4805	8.89	8.96	8.94
PKS 0112-017	46.88	...	4130	5030	...	9.21	9.36
PKS 0403-13	46.36	3735	3535	3325	8.82	8.78	8.60
PKS 0859-14	47.22	4615	3775	4520	9.46	9.29	9.40
PKS 1127-14	47.15	...	3725	3695	...	9.18	9.12
PKS 1656+053	47.06	3510	3980	...	9.13	9.22	...
PKS 2216-03	46.95	4415	3555	3600	9.35	9.14	9.04
TEX 1156+213	46.01	7740	5175	3880	9.19	8.91	8.56

^a From Runnoe et al. (2012a), all other columns from Tang et al. (2012).

hole mass because the fluxes are well known (although the uncertainty in θ is large) unless otherwise noted.

The results of the regression analysis also suggest that the H β black hole mass scaling relationship has the strongest dependence on radio core dominance, though Mg II also has a dependence, albeit weaker. Figures 3, 4, and 5 show three

combinations of difference in log of black hole mass versus $\log R$ with the regression line over-plotted. The difference $\Delta \log(M_{BH})(H\beta - \text{C IV})$ shows the steepest slope versus $\log R$, indicating that H β has the strongest bias with radio core dominance. The difference $\Delta \log(M_{BH})(\text{Mg II} - \text{C IV})$ has a slightly shallower slope, indicating that Mg II has a weaker

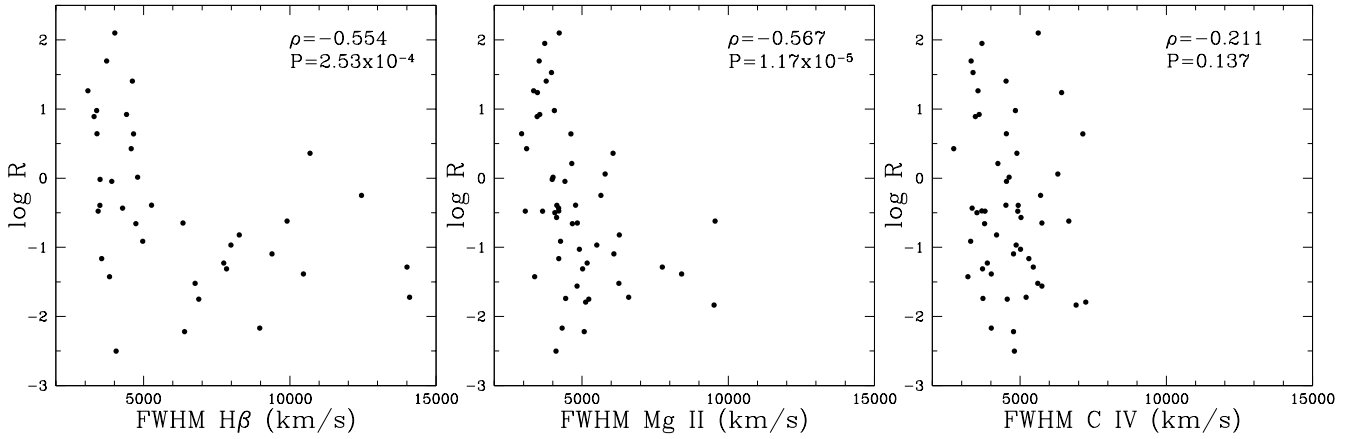


Figure 2. Radio core dominance versus FWHM for H β , Mg II, and C IV. The effect seen in Wills & Browne (1986), where large values of FWHM have small values of log R but small values of FWHM have a range of log R , is reproduced for H β and, to some extent, Mg II. This effect is not statistically significant for C IV. Spearman rank correlation coefficients (ρ) are given with the probability (P) of finding this distribution of points by chance listed underneath.

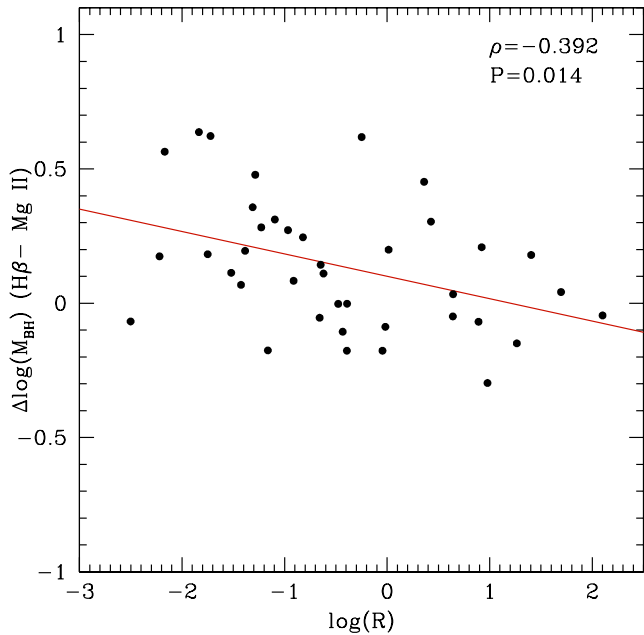


Figure 3. Log $M_{BH}(H\beta)$ –log $M_{BH}(Mg\text{ II})$ versus log R for 39 objects where measurements are available for all three quantities. The negative slope of $\Delta\log(M_{BH})(H\beta - Mg\text{ II})$ versus log R supports the conclusion that H β has the stronger dependence.

dependence on log R than does H β . The H β and Mg II-derived masses both depend on radio core dominance, but the negative slope of $\Delta\log(M_{BH})(H\beta - Mg\text{ II})$ versus log R supports the conclusion that H β has the stronger dependence.

The significance of this effect can be increased by considering the one-tailed probabilities for the correlation coefficients. Because we expect H β scaling relationships to underestimate black hole masses compared to C IV and Mg II scaling relationships for jet-on objects, we can halve the

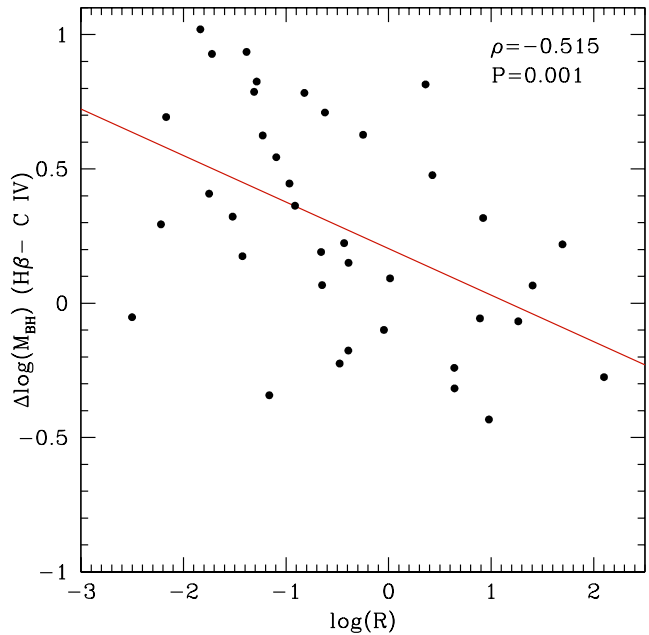


Figure 4. Log $M_{BH}(H\beta)$ –log $M_{BH}(C\text{ IV})$ versus log R for 38 objects where measurements are available for all three quantities. The solid red line shows the linear regression with a nonzero intercept. The relationship is significant at greater than the 3σ level.

probabilities given in Table 3. According to the one-tailed probabilities, the difference between the log of black hole mass versus log R is correlated with a probability of finding the observed distribution of points by chance of: < 0.7% for H β and Mg II < 0.05% for H β and C IV and < 1.1% for Mg II and C IV.

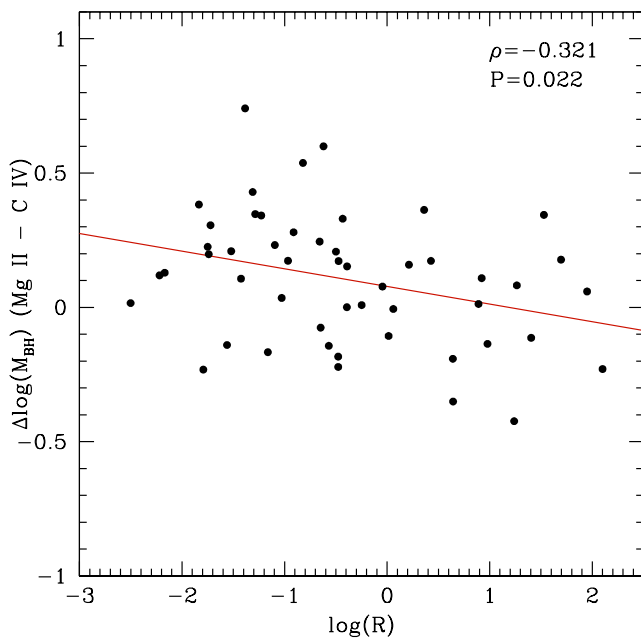


Figure 5. $\log M_{BH}(\text{Mg II}) - \log M_{BH}(\text{C IV})$ versus $\log R$ for 51 objects where measurements are available for all three quantities. The solid red line shows the linear regression with a nonzero intercept. The relationship is significant at greater than the 2σ level.

3.2.3 Luminosity considerations

In order to verify that the dependence of difference in the log of black hole masses from different scaling relationships on radio core dominance is not the result of a luminosity effect which enters via the $R - L$ relationship, we consider our sample in the luminosity- $\log R$ plane. We expect to see a slight correlation because, although the selection for similar extended luminosities means that we are looking at similar luminosity objects in principle, orientation effects are likely to introduce a trend into the observed luminosity (e.g. Nemmen & Brotherton 2010) because accretion discs are not isotropic emitters. Figure 6 shows an increase in λL_λ with radio core dominance for our objects. More face-on objects (larger $\log R$ values) have higher apparent luminosities, which will result in higher calculated black hole masses for these objects because luminosity goes to the one half power in the mass scaling relationships. We observe the Nemmen & Brotherton (2010) effect and the dependence of difference in black hole mass on radio core dominance exists in spite of it.

In principle, continuum luminosity and FWHM must both be corrected for inclination and an empirical correction to black hole mass will incorporate both dependancies, though the primary effect is derived from the FWHM dependence, which enters as the square in black hole mass scaling relationships while luminosity is only to the one half power.

In practice, we find that the empirical mass correction does not account for the luminosity dependence because we fit the correction based on the differences in the log of the black hole mass, so that the luminosity also enters as the difference, $\Delta L(5100\text{\AA} - 1450\text{\AA})$ and $\Delta L(3000\text{\AA} - 1450\text{\AA})$.

Figure 6 shows that the optical and UV luminosities have nearly the same dependence on $\log R$, so these differences are flat with radio core dominance. In order to remove the radio core dominance dependence from the luminosity for individual single-epoch mass estimates, we therefore provide corrections in Equations 2-4.

At 1450 Å:

$$\lambda L'_\lambda = \begin{cases} \lambda L_\lambda - (0.292 \pm 0.157) \log R, & \text{for } \log R \geq 0 \\ \lambda L_\lambda - (0.097 \pm 0.101) \log R, & \text{for } \log R < 0 \end{cases} \quad (2)$$

At 3000 Å:

$$\lambda L'_\lambda = \begin{cases} \lambda L_\lambda - (0.162 \pm 0.135) \log R, & \text{for } \log R \geq 0 \\ \lambda L_\lambda - (0.240 \pm 0.104) \log R, & \text{for } \log R < 0 \end{cases} \quad (3)$$

At 5100 Å:

$$\lambda L'_\lambda = \begin{cases} \lambda L_\lambda - (0.218 \pm 0.169) \log R, & \text{for } \log R \geq 0 \\ \lambda L_\lambda - (0.136 \pm 0.111) \log R, & \text{for } \log R < 0 \end{cases} \quad (4)$$

λL_λ is the uncorrected monochromatic luminosity and $\lambda L'_\lambda$ is the luminosity corrected for $\log R$. The broken fit around $\log R = 0$ is naturally motivated by the shape of the data in Figure 6.

The ratio of radio core luminosity at 5 GHz to a monochromatic optical luminosity, $\log R_V$ (different from radio loudness parameter, $\log R^*$) has been suggested to be a better indication of orientation than the radio core dominance, $\log R$, with some caveats (Wills & Brotherton 1995). As with Vestergaard et al. (2000), our result persists, but is slightly less significant, when performing the analysis with $\log R_V$ instead of $\log R$.

3.3 Correcting black hole masses for orientation

The correlations presented demonstrate a likely orientation dependence that is propagated into black hole masses calculated from $\text{H}\beta$ and Mg II FWHM measurements. The fact that no significant radio core dominance dependence is observed for the FWHM of C IV allows a correction for orientation to $\text{H}\beta$ and Mg II-derived masses. For $\text{H}\beta$, we used the fit of $\Delta \log(M_{BH})(\text{H}\beta - \text{C IV})$ versus $\log R$ to zero the difference between $\text{H}\beta$ and C IV-derived black hole masses, normalizing at $\log R = 0$. We note that other normalizations are possible, and an edge-on normalization might be preferable but is not possible here as a true edge-on view is likely obscured by a dusty torus. With the orientation dependence removed from the difference, it can be combined with the orientation unbiased C IV black hole mass estimates to give an unbiased estimate of $\text{H}\beta$ black hole mass. This process was repeated for Mg II. Equations 5 and 6 can be used to estimate black hole masses unbiased by orientation from $\text{H}\beta$ or Mg II.

$$\begin{aligned} \log \left[\frac{M_{BH}(\text{H}\beta)'}{M_\odot} \right] &= \log \left[\frac{M_{BH}(\text{H}\beta)}{M_\odot} \right] \\ &+ (0.173 \pm 0.051) \log R \end{aligned} \quad (5)$$

$$\begin{aligned} \log \left[\frac{M_{BH}(\text{Mg II})'}{M_\odot} \right] &= \log \left[\frac{M_{BH}(\text{Mg II})}{M_\odot} \right] \\ &+ (0.066 \pm 0.028) \log R \end{aligned} \quad (6)$$

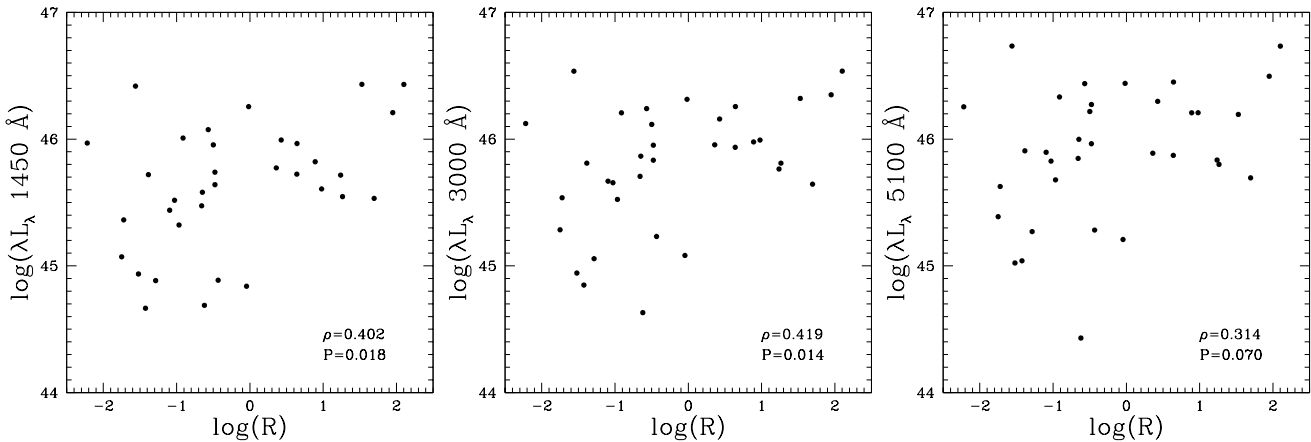


Figure 6. λL_λ at 1450, 3000, and 5100 \AA versus $\log R$. The correlations between the difference in the log of black hole mass and $\log R$ occur in spite of the correlations between λL_λ and $\log R$. The Spearman rank correlation coefficient and corresponding probability of finding this distribution of points by chance are given.

$M_{BH}(\text{H}\beta)'$ is the log of the $\text{H}\beta$ -based black hole mass with the $\log R$ dependence removed, and $M_{BH}(\text{H}\beta)$ is the log of the orientation-biased, $\text{H}\beta$ -based black hole mass estimated from the scaling relationship. The same conventions apply for Mg II . The uncertainties given here are the $1-\sigma$ errors in the fit coefficients and are not independent.

Applying this correction reduces the scatter between black hole masses estimated from different broad emission lines. The scatter around the one-to-one relationship is reduced from 0.40 dex to 0.35 dex for $\text{H}\beta$ and C IV , 0.194 dex to 0.188 dex for Mg II and C IV , and 0.20 to 0.18 for $\text{H}\beta$ and Mg II . Figures 7 and 8 show the reduction in scatter that results from applying the corrections for $\log R$ for $\text{H}\beta$ and Mg II . Original masses are shown in the left panel and corrected masses are on the right.

The caveat for these corrections is that they are linear fits to data that display a linear relationship in log space with large scatter. The errors are large due to the large scatter present in the data, and fitting with a different algorithm or prescription will yield a slightly different correction.

3.4 Radio spectral index

We repeat the analysis for radio spectral index, an orientation indicator that is more easily measured than radio core dominance because the object does not need to be resolved in the radio image. We present only the results for radio spectral index measured from all the available radio data. The results for radio spectral index measured between 1.4 and 4.9 GHz are similar, but the correlations are slightly weaker.

Radio spectral index is a good proxy for radio core dominance, the two are correlated with a probability of less than 10^{-6} for the correlation to arise by chance. Figure 9 shows radio spectral index measured from all the available radio data points versus radio core dominance. We find a best-fitting line of:

$$\alpha_{all} = (0.260 \pm 0.048) \log R - (0.433 \pm 0.048) \quad (7)$$

The orientation dependence of FWHM of $\text{H}\beta$ and Mg II

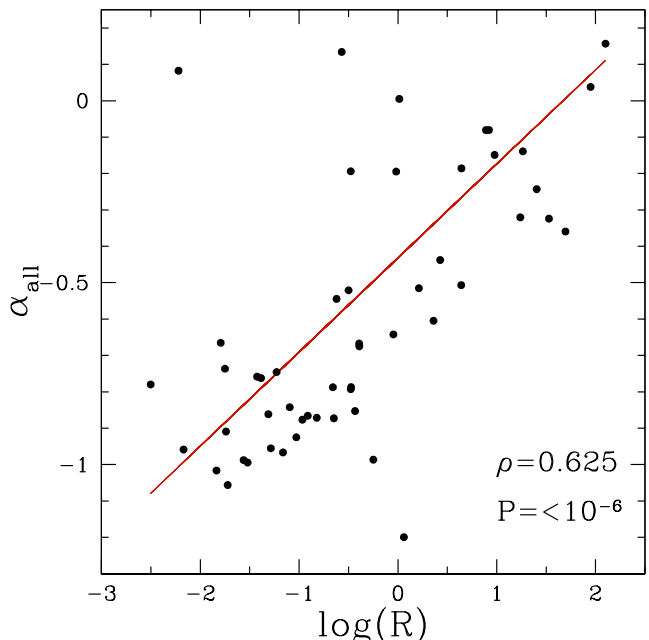


Figure 9. Radio spectral index measured for all available radio data points versus radio core dominance. α_{all} is a good proxy for $\log R$, which is traditionally used as an orientation indicator. The biggest outlier in this correlation has a spectral shape in the radio that is not well fit by a power law.

and lack of a dependence for C IV that is indicated by a radio core dominance dependence is also present for radio spectral index. Figure 10 shows this dependence on radio spectral index for all three lines.

In order to investigate how different black hole mass scaling relationships might depend on radio spectral index, we correlate it with the difference between the log of black hole masses estimated from different scaling relationships. The Spearman rank correlation coefficients and corresponding two-tailed probabilities are given in Table 3.

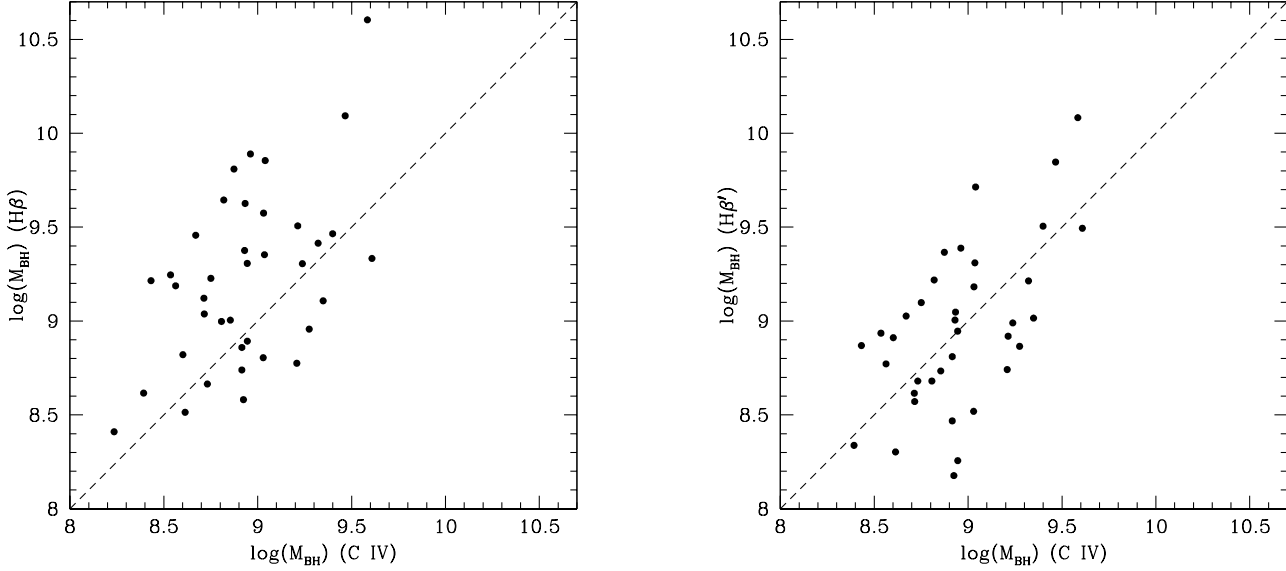


Figure 7. H β versus C IV-based black hole masses (left) and corrected H β' versus C IV-based black hole masses (right). The dashed line is the one-to-one relationship.

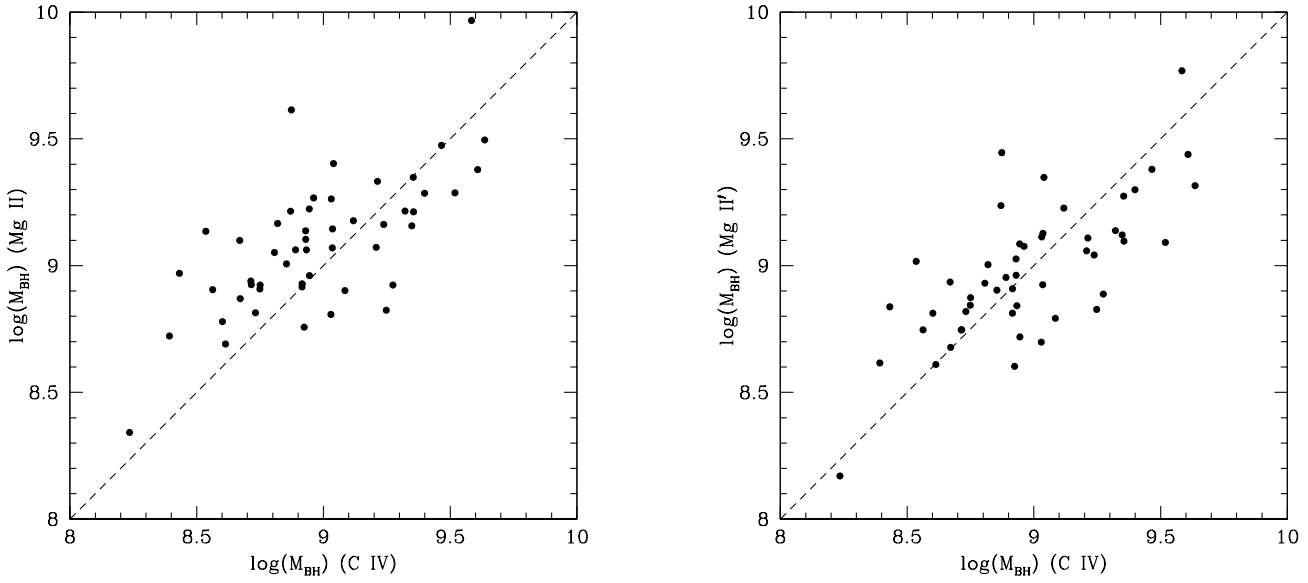


Figure 8. Mg II versus C IV-based black hole masses (left) and corrected Mg II' versus C IV-based black hole masses (right). The dashed line is the one-to-one relationship. Note that, while the reduction in scatter is modest, the points now fall more evenly around the one-to-one line.

Taking into account the number of objects available for each correlation and the probability indicated by the Spearman rank correlation test, the difference between the log of black hole masses estimated from H β and C IV, Mg II and C IV, and H β and Mg II is correlated with radio spectral index with a t-ratio of 3.3, 2.5, and 2.85, respectively. As with radio core dominance, the correlation with radio spectral index causes a range in the difference between black hole masses estimated from different emission lines that covers about an order of magnitude from the most jet-on (large values of α_{all}) to the most edge-on (small values of α_{all})

objects. Similarly, in practice, the actual range will depend on the range of orientations present in any given sample and uncertainty in the orientation from α_{all} .

We also repeated the regression analysis in order to describe the trends with radio spectral index. The uncertainties in α_{all} are considered to be negligible compared to those in black hole mass. The trends are very similar to those for radio core dominance. Figures 11, 12, and 13 show three combinations of difference in log of black hole mass versus α_{all} with the regression line over-plotted.

The behavior of the 1450, 3000, and 5100 \AA monochro-

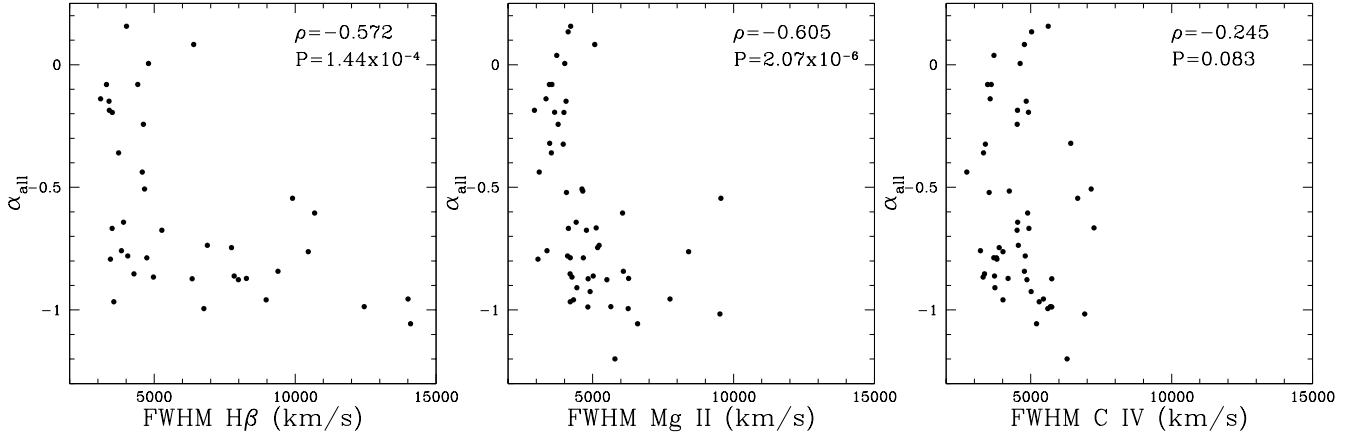


Figure 10. Radio spectral index versus FWHM for H β , Mg II, and C IV. The effect seen with radio core dominance is reproduced for radio spectral index. Spearman rank correlation coefficients are given with the probability of finding this distribution of points by chance listed underneath.

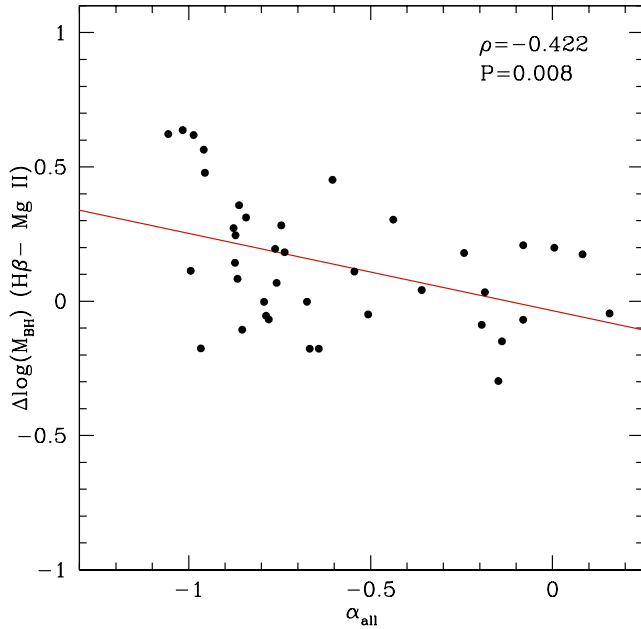


Figure 11. $\log M_{BH}(H\beta) - \log M_{BH}(Mg\text{ II})$ versus radio spectral index for 39 objects where measurements are available for all three quantities. The solid red line shows the linear regression with a nonzero intercept. The relationship is significant at approximately the 3σ level.

matic luminosities with radio spectral index is similar as for radio core dominance. The differences in luminosity are not correlated with α_{all} but the individual luminosities are, so we provide a correction to these that should be applied before calculating black hole masses from the single-epoch scaling relationships. There is no evidence in Figure 14 that a broken fit is necessary here, so we fit only one line. The data have a lot of irregular scatter and we find that assuming the errors in radio spectral index are negligible and weighting all the monochromatic luminosities similarly gives

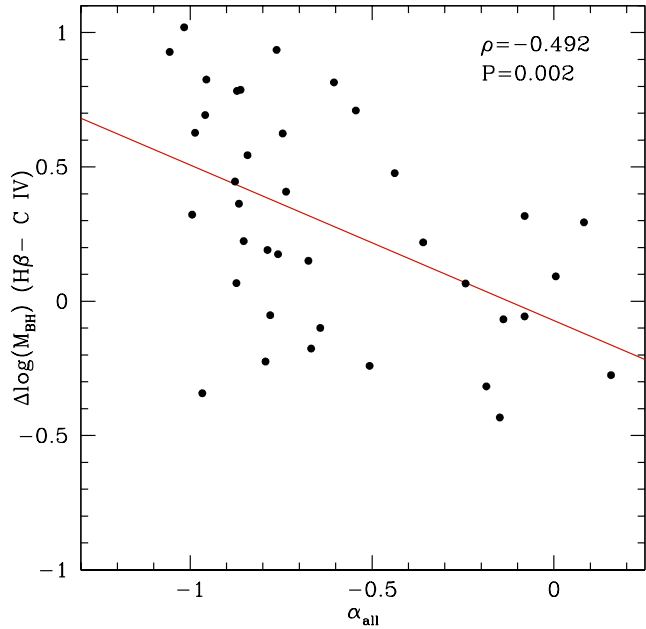


Figure 12. $\log M_{BH}(H\beta) - \log M_{BH}(C\text{ IV})$ versus radio spectral index for 38 objects where measurements are available for all three quantities. The solid red line shows the linear regression with a nonzero intercept. The relationship is significant at greater than the 3σ level.

the best fit. We normalize the correction at $\alpha_{all} = -0.432$, which corresponds to $\log R = 0$ in Equation 7.

At 1450 Å:

$$\lambda L'_\lambda = \lambda L_\lambda - (0.716 \pm 0.202) \alpha_{all} - (0.310 \pm 0.211) \quad (8)$$

At 3000 Å:

$$\lambda L'_\lambda = \lambda L_\lambda - (0.678 \pm 0.201) \alpha_{all} - (0.293 \pm 0.210) \quad (9)$$

At 5100 Å:

$$\lambda L'_\lambda = \lambda L_\lambda - (0.675 \pm 0.222) \alpha_{all} - (0.292 \pm 0.229) \quad (10)$$

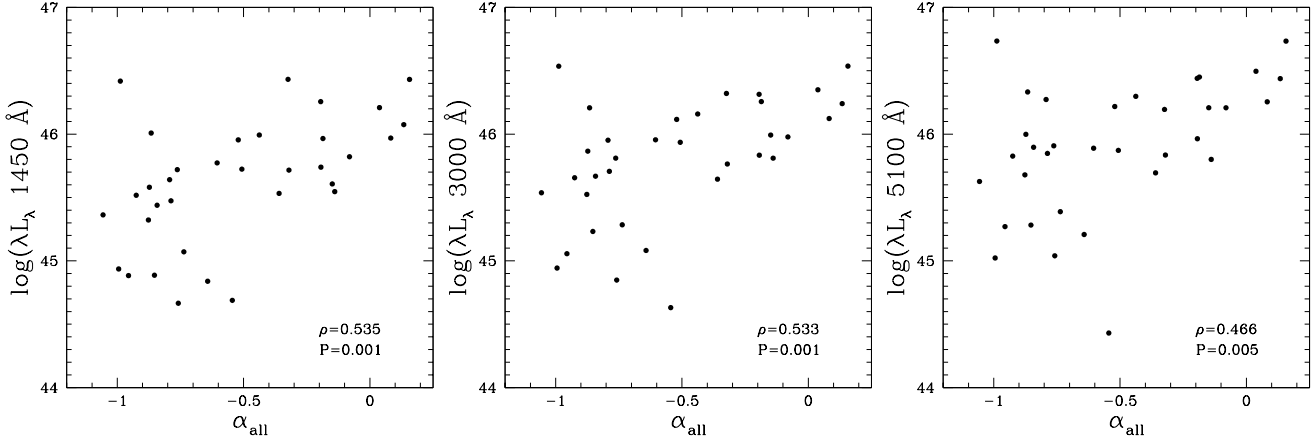


Figure 14. λL_λ at 1450, 3000, and 5100 Å versus α_{all} . The correlations between black hole mass difference and α_{all} occur in spite of the correlations between λL_λ and α_{all} . The Spearman rank correlation coefficient and corresponding probability of finding this distribution of points by chance are given.

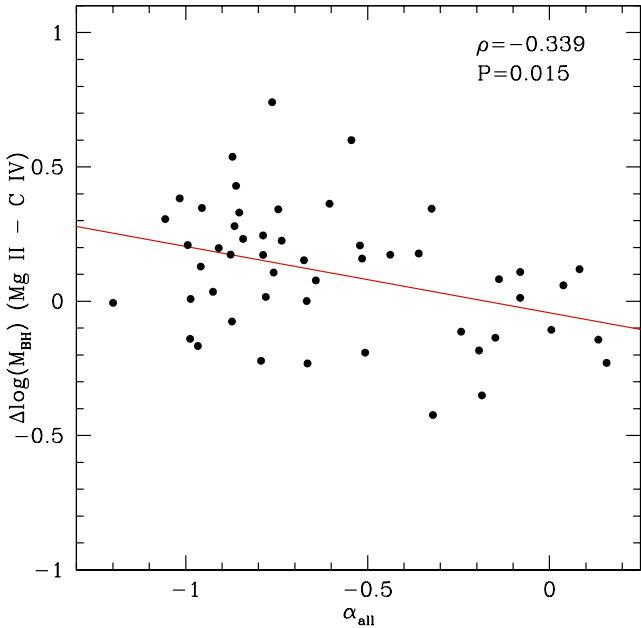


Figure 13. Log $M_{BH}(\text{Mg II}) - \log M_{BH}(\text{C IV})$ versus radio spectral index for 51 objects where measurements are available for all three quantities. The solid red line shows the linear regression with a nonzero intercept. The relationship is significant at nearly the 3 σ level.

λL_λ is the uncorrected monochromatic luminosity and $\lambda L'_\lambda$ is the luminosity corrected for α_{all} .

The regression and correlation analysis with radio spectral index indicate that a likely orientation dependence is propagated into black hole masses calculated from H β and Mg II FWHM measurements and we again provide a correction for this effect. We use the fits of $\Delta \log(M_{BH})(\text{H}\beta - \text{C IV})$ and $\Delta \log(M_{BH})(\text{Mg II} - \text{C IV})$ to zero the α_{all} dependence, normalizing to $\alpha_{all} = -0.432$. Using the same methodology as for radio core dominance, we arrive at the following

corrections for black hole mass in terms of radio spectral index:

$$\log \left[\frac{M_{BH}(\text{H}\beta)'_\alpha}{M_\odot} \right] = \log \left[\frac{M_{BH}(\text{H}\beta)}{M_\odot} \right] + (0.580 \pm 0.170) \alpha_{all} + (0.251 \pm 0.180) \quad (11)$$

$$\log \left[\frac{M_{BH}(\text{Mg II})'_\alpha}{M_\odot} \right] = \log \left[\frac{M_{BH}(\text{Mg II})}{M_\odot} \right] + (0.247 \pm 0.088) \alpha_{all} + (0.107 \pm 0.106) \quad (12)$$

$M_{BH}(\text{H}\beta)'_\alpha$ is the log of the H β -based black hole mass with the α_{all} dependence removed, and $M_{BH}(\text{H}\beta)$ is the log of the orientation-biased, H β -based black hole mass estimated from the scaling relationship. The same conventions apply for Mg II. The uncertainties given here are the 1- σ errors in the fit coefficients and are not independent.

Applying this correction reduces the scatter between black hole masses estimated from different broad emission lines. The scatter around the one-to-one relationship is reduced from 0.40 dex to 0.35 dex for H β and C IV, 0.194 dex to 0.188 dex for Mg II and C IV, and 0.20 to 0.18 for H β and Mg II. To the number of decimal places shown, the reduction in scatter is exactly the same as for $\log R$. Figures 15 and 16 show the reduction in scatter that results from applying the corrections for α_{all} for H β and Mg II. Original masses are shown in the left panel and corrected masses are on the right.

4 DISCUSSION

We correlated differences in the log of black hole mass estimates with the orientation indicators radio core dominance and radio spectral index. We found that the dependence of FWHM of H β and Mg II $\lambda 2798$ on orientation indicators propagates into black hole masses estimated from scaling relationships based on these emission lines, and derived corrections to H β and Mg II black hole masses for this effect. The orientation indicator dependence is strongest for the black hole masses based on measurements of H β FWHM,

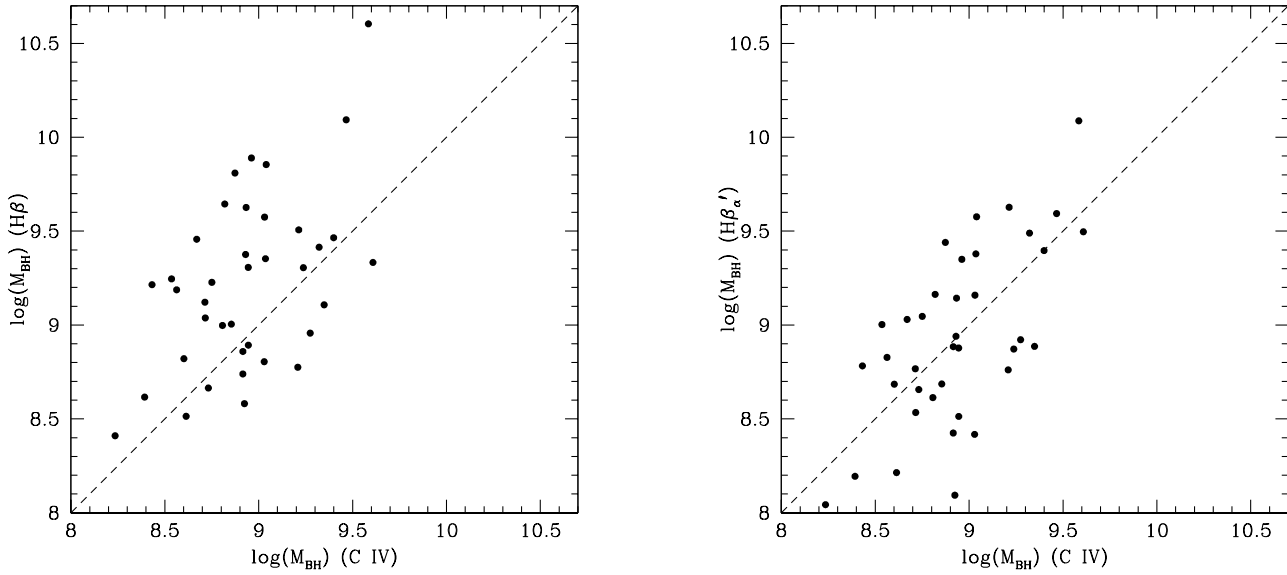


Figure 15. H β versus C IV-based black hole masses (left) and radio spectral index corrected H β'_α versus C IV-based black hole masses (right). The dashed line is the one-to-one relationship.

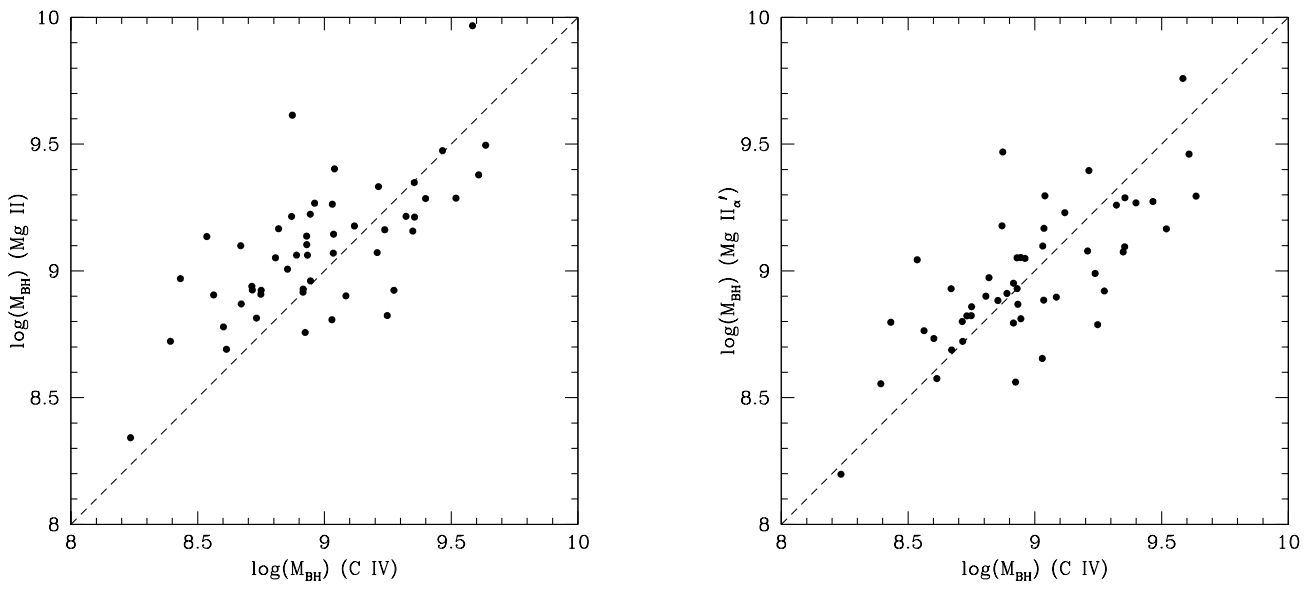


Figure 16. Mg II versus C IV-based black hole masses (left) and radio spectral index corrected Mg II'_ α versus C IV-based black hole masses (right). The dashed line is the one-to-one relationship. Note that, while the reduction in scatter is modest, the points now fall more evenly around the one-to-one line.

although differences associated with Mg II-based measurements also show some dependence.

The range in the difference between black hole masses estimated from different emission lines covers nearly an order of magnitude from edge-on to jet-on, although it will depend on the orientation biases in any given sample. Note that this sample was originally selected to have a full range in $\log R$ and will likely have a different distribution of orientations than a flux limited or randomly selected sample.

Because of the nature of the broad-lined objects in our sample, “edge-on” will likely be closer to 45° than 90°

(Barthel 1989). If quasars could be observed at a true edge-on inclination, we might expect to measure an even broader FWHM and estimate a correspondingly larger black hole mass. The scale factor f derived from such a mass might be closer to unity than the larger statistical values that are currently available, implying that the current value is inflated to compensate for orientation and projection effects.

Radio core dominance and radio spectral index are indicators of inclination angle and, while the measurement uncertainties on $\log R$ and α_{all} are relatively low, converting to θ will introduce additional scatter. The exact amount is

model dependent, but at least in the case of Ghisellini et al. (1993), the scatter is substantial. The implication for this analysis is that the correction to $H\beta$ and $Mg\text{ II}$ black hole masses were derived from a fitting procedure that assumed negligible uncertainty in $\log R$ compared to the uncertainty in black hole mass. A physical correction for inclination angle would require another fitting procedure that assumes uncertainty in both parameters. We provide only the corrections for $\log R$ and α_{all} as they are model independent and more useful in practice.

Given the size and significance of the R -dependence of black hole mass scaling relationships, it would be advisable to recalibrate them with the radio core dominance dependence taken into account. The $H\beta$ scaling relationship is based on reverberation mapping of the $H\beta$ line, so this entails doing reverberation mapping on RL objects and also obtaining UV spectra and assuming that the BLR is the same in RL and radio-quiet objects. Ideally this would be done for a large sample of RL quasars with known orientations, although few of these have been done. These new orientation-independent single-epoch mass scaling relationships would be useful for the $\sim 10\%$ of quasars that are RL. They must also have high-quality radio maps for measuring $\log R$ which becomes more difficult with increasing redshift for a number of reasons. This could also be done with radio spectral index which is easier to measure and can be measured for some objects in which $\log R$ cannot.

While the C IV scaling relationship does not itself depend on orientation, its original calibration has scatter from orientation effects and should be corrected. C IV and $Mg\text{ II}$ scaling relationships are based on reverberation mapping of $H\beta$ (Vestergaard & Peterson 2006; Vestergaard & Osmer 2009) that shows a radio core dominance dependence. Recalibrating the C IV and $Mg\text{ II}$ scaling relationships with this effect taken into account should reduce their scatter.

When black hole mass scaling relationships are re-derived, they should also be cast in terms of the line dispersion, σ_{line} . The parameter σ_{line} is the “best” line width measure for deriving black hole mass in the sense that it gives the least biased result (Peterson 2011). There is a larger range in FWHM than σ_{line} and, since the measure of line width is squared in scaling relationships, the extreme values possible for FWHM will introduce a larger range in black hole mass. If the black hole mass scaling relationships are re-cast in a consistent way for line dispersion as well as FWHM, then the σ_{line} -based scaling relationships can be explored to see if they are more robust than FWHM against radio core dominance and radio spectral index.

It has been argued that C IV may not be an appropriate choice for estimating black hole mass from a single-epoch spectrum because there may be a strong wind component and the motions of the C IV gas may not be dominated by gravity (e.g., Dunlop 2004; Bachev et al. 2004; Shemmer et al. 2004; Baskin & Laor 2005). This is likely the case in many narrow-line Seyfert 1 galaxies that exhibit the characteristic triangular profile indicative of an outflowing wind and the black hole mass scaling relationships do not apply to these objects (none of the objects in this sample have such a line profile for C IV .) Quasars do not share these types of asymmetric profiles, but their profiles are often blueshifted relative to the systemic redshift of the object (Wilkes 1984). The objects with the largest

C IV blueshifts exhibit broader lines (Brotherton et al. 1994; Richards et al. 2002; Ho et al. 2012), but the corresponding increase in black hole mass is small, well within the uncertainty in the mass estimate. Despite these issues, it is not clear that C IV is any less trustworthy of a black hole mass indicator than $H\beta$ or $Mg\text{ II}$, which also have problems (Vestergaard et al. 2011; Assef et al. 2011). Reverberation mapping on C IV shows a virial relationship (Peterson & Wandel 1999, 2000; Vestergaard et al. 2011; Peterson 2011) and there are a number of advantages to using the C IV line (Vestergaard & Peterson 2006; Warner et al. 2003; Vestergaard 2002). Most importantly for this study, C IV is not biased by orientation as measured by radio core dominance or radio spectral index as are other lines. The lack of a significant radio core dominance dependence for C IV FWHM may be due to the fact that there is a component to the line that does not reverberate (Denney 2012), if the reverberating component could be isolated one might expect it to behave more like the $H\beta$ line.

The correction for orientation, as indicated by radio core dominance and radio spectral index, is only one of a suite of corrections that will reduce the scatter in black hole mass scaling relationships. Assef et al. (2011) perform a study similar to this one on a sample of 12 high-redshift, gravitationally lensed quasars. They specifically compare black hole masses based on C IV to those from $H\beta$ and $H\alpha$ and find that the residuals between the C IV -based masses and the $H\beta$ or $H\alpha$ -based masses correlate with the ratio of the UV to optical continuum luminosities. A correction based on this color dependence reduces the scatter in the residuals by almost a factor of two. Additional sources of scatter in the black hole mass scaling relationships include the role of radiation pressure in determining the line profile (e.g., Marconi et al. 2008), Eddington ratio (Onken & Kollmeier 2008), uncertainties from source variability (Woo & Park 2011), and effects of low S/N data and measurement uncertainties (Denney et al. 2011). While our result is based only on RL quasars, it may be true of RQ quasars as well (as shown by Jarvis & McLure 2006). If orientation indicators, like that of Boroson (2011), are developed for RQ quasars, this effect can be investigated and possibly used to further reduce the scatter in scaling relationships.

5 CONCLUSIONS

Using the RL subsample of the Shang et al. (2011) SED atlases, we have analyzed the dependence on radio core dominance and radio spectral index for differences in the log of black hole masses estimated from self-consistent scaling relationships and quasi-simultaneous optical-UV data for $H\beta$, $Mg\text{ II}$, and C IV . We correlated the difference between the log of black hole masses estimated from these lines with orientation indicators and found that $H\beta$ and $Mg\text{ II}$ -based masses are biased with respect to radio core dominance and radio spectral index as compared to masses estimated from C IV . The dependence is such that $H\beta$ and $Mg\text{ II}$ will underestimate black hole mass compared to C IV for jet-on objects, the effect is stronger for $H\beta$, and the range in the difference between black hole masses estimated from different emission lines covers nearly an order of magnitude in black hole mass

from our most jet-on to edge-on objects. We used the C IV FWHM-based mass estimates, unbiased with respect to radio core dominance and radio spectral index, to derive the following corrections for black hole masses based on H β and Mg II FWHM in terms of log R and α_{all} :

$$\log \left[\frac{M_{BH}(\text{H}\beta)'}{M_{\odot}} \right] = \log \left[\frac{M_{BH}(\text{H}\beta)}{M_{\odot}} \right] + (0.173 \pm 0.051) \log R \quad (13)$$

$$\log \left[\frac{M_{BH}(\text{Mg II})'}{M_{\odot}} \right] = \log \left[\frac{M_{BH}(\text{Mg II})}{M_{\odot}} \right] + (0.066 \pm 0.028) \log R \quad (14)$$

$$\log \left[\frac{M_{BH}(\text{H}\beta)'_{\alpha}}{M_{\odot}} \right] = \log \left[\frac{M_{BH}(\text{H}\beta)}{M_{\odot}} \right] + (0.580 \pm 0.170) \alpha_{all} + (0.251 \pm 0.180) \quad (15)$$

$$\log \left[\frac{M_{BH}(\text{Mg II})'_{\alpha}}{M_{\odot}} \right] = \log \left[\frac{M_{BH}(\text{Mg II})}{M_{\odot}} \right] + (0.247 \pm 0.088) \alpha_{all} + (0.107 \pm 0.106) \quad (16)$$

When the log R corrections are applied, scatter around the one-to-one relationship is reduced from 0.40 to 0.35 dex between H β and C IV-based black hole masses, 0.194 to 0.188 dex for Mg II and C IV, and 0.20 to 0.18 dex for H β and Mg II. The scatter reduction is the same when using corrections based on radio spectral index.

We investigated the role of luminosity in the correlation between differences in the log of black hole mass and orientation indicators and found that differences in luminosity do not depend on radio core dominance or radio spectral index and are therefore not being corrected in our empirical corrections. The individual luminosities at 1450, 3000, and 5100 Å do depend on the orientation indicators so we provide separate corrections that are to be applied to the luminosity before calculating black hole mass from the single-epoch scaling relationships:

At 1450 Å:

$$\lambda L'_{\lambda} = \begin{cases} \lambda L_{\lambda} - (0.292 \pm 0.157) \log R, & \text{for } \log R \geq 0 \\ \lambda L_{\lambda} - (0.097 \pm 0.101) \log R, & \text{for } \log R < 0 \end{cases} \quad (17)$$

$$\lambda L'_{\lambda} = \lambda L_{\lambda} - (0.716 \pm 0.202) \alpha_{all} - (0.310 \pm 0.211) \quad (18)$$

At 3000 Å:

$$\lambda L'_{\lambda} = \begin{cases} \lambda L_{\lambda} - (0.162 \pm 0.135) \log R, & \text{for } \log R \geq 0 \\ \lambda L_{\lambda} - (0.240 \pm 0.104) \log R, & \text{for } \log R < 0 \end{cases} \quad (19)$$

$$\lambda L'_{\lambda} = \lambda L_{\lambda} - (0.678 \pm 0.201) \alpha_{all} - (0.293 \pm 0.210) \quad (20)$$

At 5100 Å:

$$\lambda L'_{\lambda} = \begin{cases} \lambda L_{\lambda} - (0.218 \pm 0.169) \log R, & \text{for } \log R \geq 0 \\ \lambda L_{\lambda} - (0.136 \pm 0.111) \log R, & \text{for } \log R < 0 \end{cases} \quad (21)$$

$$\lambda L'_{\lambda} = \lambda L_{\lambda} - (0.675 \pm 0.222) \alpha_{all} - (0.292 \pm 0.229) \quad (22)$$

This type of correction is only one of a suite of many corrections that will tighten the black hole mass scaling relationships. By tracking down additional physical parameters

that affect mass estimates and searching for new correlations, we can reduce the scatter in the scaling relationships even further.

ACKNOWLEDGMENTS

J. Runnoe would like to thank Hannah Jang-Condell for her support and Sabrina Cales and Adam Myers for helpful discussions.

This work funded by Wyoming NASA Space Grant Consortium, NASA Grant #NNX10A095H.

REFERENCES

Assef R. J., Denney K. D., Kochanek C. S., Peterson B. M., Kozłowski S., Ageorges N., Barrows R. S., Buschkamp et al., 2011, ApJ, 742, 93
 Assef R. J., Frank S., Grier C. J., Kochanek C. S., Denney K. D., Peterson B. M., 2012, eprint arXiv:1203.2617
 Bachev R., Marziani P., Sulentic J. W., Zamanov R., Calvani M., Dultzin Hacyan D., 2004, ApJ, 617, 171
 Barthel P. D., 1989, ApJ, 336, 606
 Baskin A., Laor A., 2005, MNRAS, 356, 1029
 Becker R. H., White R. L., Helfand D. J., 1995, ApJ, 450, 559
 Bentz M. C., Walsh J. L., Barth A. J., Baliber N., Bennert V. N., Canalizo G., Filippenko A. V., Ganeshalingam M., et al., 2009, ApJ, 705, 199
 Bentz M. C., Walsh J. L., Barth A. J., Baliber N., Bennert V. N., Canalizo G., Filippenko A. V., Ganeshalingam M., et al., 2009, ApJ, 705, 199
 Blandford R. D., McKee C. F., 1982, ApJ, 255, 419
 Boroson T. A., 2011, ApJL, 735, L14
 Boroson T. A., Green R. F., 1992, ApJ, 80, 109
 Brotherton M. S., 1996, ApJS, 102, 1
 Brotherton M. S., Wills B. J., Francis P. J., Steidel C. C., 1994, ApJ, 430, 495
 Collin S., Kawaguchi T., Peterson B. M., Vestergaard M., 2006, A&Ap, 456, 75
 Cooper N. J., Lister M. L., Kochaneczyk M. D., 2007, ApJS, 171, 376
 Dennett-Thorpe J., Bridle A. H., Scheuer P. A. G., Laing R. A., Leahy J. P., 1997, MNRAS, 289, 753
 Denney K., Assef R. J., Bentz M., Dietrich M., Horne K., Kochanek C. S., Mathur S., Peterson B. M., et al., 2011, in Narrow-Line Seyfert 1 Galaxies and their Place in the Universe Addressing systematic uncertainties in black hole mass measurements
 Denney K. D., 2012, ArXiv e-prints
 DiPompeo M. A., Brotherton M. S., De Breuck C., 2012, ApJ, 752, 6
 Dunlop J. S., 2004, Coevolution of Black Holes and Galaxies, p. 341
 Fey A. L., Charlot P., 2000, ApJS, 128, 17
 Fine S., Jarvis M. J., Mauch T., 2011, MNRAS, 412, 213
 Ghisellini G., Padovani P., Celotti A., Maraschi L., 1993, ApJ, 407, 65
 Gilbert G. M., Riley J. M., Hardcastle M. J., Croston J. H., Pooley G. G., Alexander P., 2004, MNRAS, 351, 845

Grier C. J., Peterson B. M., Pogge R. W., Denney K. D., Bentz M. C., Martini P., Sergeev S. G., Kaspi S., et al., 2012, *ApJ*, 755, 60

Ho L. C., Goldoni P., Dong X.-B., Greene J. E., Ponti G., 2012, *ApJ*, 754, 11

Hutchings J. B., Gower A. C., Ryneveld S., Dewey A., 1996, *AJ*, 111, 2167

Hutchings J. B., Price R., Gower A. C., 1988, *ApJ*, 329, 122

Jarvis M. J., McLure R. J., 2006, *MNRAS*, 369, 182

Kaspi S., Brandt W. N., Maoz D., Netzer H., Schneider D. P., Shemmer O., 2007, *ApJ*, 659, 997

Kaspi S., Maoz D., Netzer H., Peterson B. M., Vestergaard M., Jannuzzi B. T., 2005, *ApJ*, 629, 61

Kaspi S., Smith P. S., Netzer H., Maoz D., Jannuzzi B. T., Giveon U., 2000, *ApJ*, 533, 631

Kellermann K. I., Sramek R., Schmidt M., Shaffer D. B., Green R., 1989, *AJ*, 98, 1195

Kovalev Y. Y., Kellermann K. I., Lister M. L., Homan D. C., Vermeulen R. C., Cohen M. H., Ros E., Kadler M., Lobanov A. P., Zensus J. A., Kardashev N. S., Gurvits L. I., Aller M. F., Aller H. D., 2005, *AJ*, 130, 2473

Kriss G., 1994, *Astronomical Data Analysis Software and Systems*, 3, 437

Lister M. L., Gower A. C., Hutchings J. B., 1994, *AJ*, 108, 821

McLure R. J., Dunlop J. S., 2001, *MNRAS*, 327, 199

Marconi A., Axon D. J., Maiolino R., Nagao T., Pastorini G., Pietrini P., Robinson A., Torricelli G., 2008, *ApJ*, 678, 693

Markwardt C. B., 2009, in D. A. Bohlender, D. Durand, & P. Dowler ed., *Astronomical Data Analysis Software and Systems XVIII* Vol. 411 of *Astronomical Society of the Pacific Conference Series*, Non-linear Least-squares Fitting in IDL with MPFIT. p. 251

Miley G. K., Hartsuijker A. P., 1978, *A&ApS*, 34, 129

Mullin L. M., Hardcastle M. J., Riley J. M., 2006, *MNRAS*, 372, 113

Nemmen R. S., Brotherton M. S., 2010, *MNRAS*, 408, 1598

Netzer H., Brotherton M. S., Wills B. J., Han M., Wills D., Baldwin J. A., Ferland G. J., Browne I. W. A., 1995, *ApJ*, 448, 27

Onken C. A., Kollmeier J. A., 2008, *ApJL*, 689, L13

Orr M. J. L., Browne I. W. A., 1982, *MNRAS*, 200, 1067

Peterson B. M., 1993, *PASP*, 105, 247

Peterson B. M., 2011, arXiv, astro-ph.CO, 4181

Peterson B. M., Ferrarese L., Gilbert K. M., Kaspi S., Malkan M. A., Maoz D., Merritt D., Netzer H., et al., 2004, *ApJ*, 613, 682

Peterson B. M., Wandel A., 1999, *ApJL*, 521, L95

Peterson B. M., Wandel A., 2000, *ApJL*, 540, L13

Reid A., Shone D. L., Akujor C. E., Browne I. W. A., Murphy D. W., Pedelty J., Rudnick L., Walsh D., 1995, *A&ApS*, 110, 213

Reid R. I., Kronberg P. P., Perley R. A., 1999, *ApJS*, 124, 285

Richards G. T., Vanden Berk D. E., Reichard T. A., Hall P. B., Schneider D. P., SubbaRao M., Thakar A. R., York D. G., 2002, *AJ*, 124, 1

Rogora A., Padrielli L., de Ruiter H. R., 1986, *A&ApS*, 64, 557

Runnoe J. C., Brotherton M. S., Shang Z., 2012a, *MNRAS*, 422, 478

Runnoe J. C., Brotherton M. S., Shang Z., 2012b, ArXiv e-prints

Scheuer P. A. G., Readhead A. C. S., 1979, *Nature*, 277, 182

Scott W. K., Fomalont E. B., Horiuchi S., Lovell J. E. J., Moellenbrock G. A., Dodson R. G., Edwards P. G., Coldwell G. V., et al., 2004, *ApJS*, 155, 33

Shang Z., Brotherton M. S., Wills B. J., Wills D., Cales S. L., Dale D. A., Green R. F., Runnoe J. C., et al., 2011, *ApJS*, 196, 2

Shang Z., Wills B. J., Wills D., Brotherton M. S., 2007, *ApJ*, 134, 294

Shemmer O., Netzer H., Maiolino R., Oliva E., Croom S., Corbett E., di Fabrizio L., 2004, *ApJ*, 614, 547

Spencer R. E., Schilizzi R. T., Fanti C., Fanti R., Parma P., van Breugel W. J. M., Venturi T., Muxlow T. W. B., Rendong N., 1991, *MNRAS*, 250, 225

Stanghellini C., O'Dea C. P., Dallacasa D., Cassaro P., Baum S. A., Fanti R., Fanti C., 2005, *A&Ap*, 443, 891

Stocke J. T., Morris S. L., Weymann R. J., Foltz C. B., 1992, *ApJ*, 396, 487

Tang B., Shang Z., Brotherton M. S., Runnoe J. C., 2012, *ApJ*

Vestergaard M., 2002, *ApJ*, 571, 733

Vestergaard M., Denney K., Fan X., Jensen J. J., Kelly B. C., Osmer P. S., Peterson B. M., Tremonti C. A., 2011, *Narrow-Line Seyfert 1 Galaxies and their Place in the Universe*, -1, 38

Vestergaard M., Osmer P. S., 2009, arXiv, astro-ph.CO

Vestergaard M., Peterson B. M., 2006, *ApJ*, 641, 689

Vestergaard M., Wilkes B. J., 2001, *ApJS*, 134, 1

Vestergaard M., Wilkes B. J., Barthel P. D., 2000, *ApJ*, 538, L103

Warner C., Hamann F., Dietrich M., 2003, *ApJ*, 596, 72

Wilkes B. J., 1984, *MNRAS*, 207, 73

Wills B. J., Brotherton M. S., 1995, *ApJ*, 448, L81

Wills B. J., Browne I. W. A., 1986, *ApJ*, 302, 56

Wills B. J., Netzer H., Brotherton M. S., Han M., Wills D., Baldwin J. A., Ferland G. J., Browne I. W. A., 1993, *ApJ*, 410, 534

Wills B. J., Thompson K. L., Han M., Netzer H., Wills D., Baldwin J. A., Ferland G. J., Browne I. W. A., Brotherton M. S., 1995, *ApJ*, 447, 139

Woo J. H., Park D., 2011, in *Narrow-Line Seyfert 1 Galaxies and their Place in the Universe* The overall uncertainty of single-epoch virial black hole mass estimators and its implication to the M-sigma relation

Woo J.-H., Treu T., Barth A. J., Wright S. A., Walsh J. L., Bentz M. C., Martini P., Bennert V. N., Canalizo G., Filippenko A. V., Gates E., Greene J., Li W., Malkan M. A., Stern D., Minezaki T., 2010, *ApJ*, 716, 269